Surveys in Geophysics manuscript No.
(will be inserted by the editor)

The representation of tropospheric water vapor over low-latitude oceans in (re-)analysis

Errors, impacts, and the ability to exploit current and prospective observations

Robert Pincus · Anton Beljaars · Stefan A. Buehler · Gottfried Kirchengast · Florian Ladstaedter · Jeffrey S. Whitaker

Received: date / Accepted: date

Abstract This paper addresses the representation of lower tropospheric water vapor in the meteorological analyses – fully-detailed estimates of atmospheric state – providing the wide temporal and spatial coverage used in many process studies. Analyses are produced in a cycle combining short forecasts from initial conditions with data assimilation that optimally estimates the state of the atmosphere from the previous forecasts and new observations, providing initial conditions for the next set of forecasts. Estimates of water vapor are among the less certain aspects of the state because the quantity poses special challenges for data assimilation while being particularly sensitive to the details of model parameterizations. Over remote tropical oceans observations of water vapor come from two sources: passive observations at microwave or infrared wavelengths that provide relatively strong constraints over large areas on column-integrated moisture but relatively coarse vertical resolution, and occultations

Robert Pincus
Cooperative Institute for Research in Environmental Sciences, University of Colorado, and
NOAA Earth System Research Lab, Physical Sciences Division
Boulder, Colorado, USA
E-mail: Robert.Pincus@colorado.edu

Anton Beljaars
European Centre for Medium-Range Weather Forecasts
Shinfield Park, Reading, UK

Stefan A. Buehler
Universitt Hamburg, Faculty of Mathematics, Informatics and Natural Sciences
Department of Earth Sciences, Meteorological Institute,
Bundesstrae 55, 20146 Hamburg, Germany

Gottfried Kirchengast · Florian Ladstaedter
Wegener Center for Climate and Global Change and
Institute for Geophysics, Astrophysics, and Meteorology/Institute of Physics,
University of Graz, Graz, Austria

Jeffrey S. Whitaker
NOAA Earth System Research Lab, Physical Sciences Division
Boulder, Colorado, USA

of Global Positioning System provide much higher accuracy and vertical resolution but are relatively spatially coarse. Over low-latitude oceans, experiences with two systems suggest that current analyses reproduce much of the large-scale variability in integrated water vapor but have systematic errors in the representation of the boundary layer with compensating errors in the free troposphere; these errors introduce errors of order 10% in radiative heating rates through the free troposphere. New observations, such as might be obtained by future observing systems, improve the estimates of water vapor but this improvement is lost relatively quickly, suggesting that exploiting better observations will require targeted improvements to global forecast models.

Keywords Water vapor · satellite · microwave · infrared · radio occultation · data assimilation · tropospheric water vapor profiling

1 Tropospheric water vapor over low-latitude oceans

The vertical distribution of water vapor in the troposphere, through its influence on shallow and deep convection (see Mapes et al., this issue), controls many aspects of tropical climate. The distribution is tightly coupled to the processes underlying the self-aggregation of convection (Wing et al, 2017). Through its influence on radiative cooling rates the distribution of water vapor largely controls the amount of large-scale subsidence and hence the structure of thermal and moisture inversions to which the properties of low clouds are so sensitive, so the distribution plays an important role in determining low cloud feedbacks on climate change (Klein et al., this issue; Vial et al (2017)).

How can the distribution of water vapor be determined? Observations from field campaigns, including high-density dropsonde deployments (Stevens et al, 2017) or results from specialized remote sensing instruments on airborne platforms (Kiemle et al., this issue) provide the detail needed to spark and test hypothesis. Many studies, however, require observations with more uniform sampling across broader spatial and temporal scales (i.e. Lebsock et al., this issue and the studies reviewed by Klein et al., this issue). Retrievals based on measurements from microwave or infrared sounding instruments provide one possible source of observations for water vapor (see the use in Lebsock et al., this issue). An alternative is to include the same observations, or a subset thereof, in the construction of meteorological analyses. The two approaches are more similar than is immediately obvious (Parker, 2016): both use radiative transfer models and prior knowledge of the likely state of the atmosphere to provide more refined estimates of water vapor concentrations. As we will show, analyses can be compromised by errors in the model used to produce short-term forecasts, but are enhanced by the use of a wide range of observations and by the influence of recent observations on the initial estimate of atmospheric state.

Here we assess the current state of routine knowledge of lower tropospheric water vapor over remote tropical oceans. We describe how observations are synthesized in time and space to produce meteorological analyses and discuss the two broad classes of observations – multi- or hyper-spectral sounding and radio occultation – that inform these estimates in current analysis systems. The representation of water vapor

over remote low-latitude oceans in two analysis systems is compared to independent observations in regimes spanning a range of convective depth. In both systems the representation of boundary layer humidity is biased, resulting in compensating errors in the free troposphere; these errors lead to errors of order 10% in radiative heating rates in the free troposphere. Data assimilation experiments suggest that even substantially richer observational capabilities will need to be paired with systematic model improvements in order to realize more accurate estimates of boundary-layer humidity.

2 Integrating observations in space and time: data assimilation and (re-)analysis

2.1 Producing meteorological (re-)analyses

In the context of this paper an atmospheric analysis is an estimate of the instantaneous state of the atmosphere in which all state variables are defined at every location. The skill of current analyses is due to their use as initial conditions for numerical weather prediction (NWP): accurate forecasts require accurate initial conditions, so NWP centers invest heavily in all aspect of analysis production including quality control, bias correction, and the use of as many observations and observation types as possible. Given our focus on lower tropospheric moisture analysis over tropical ocean our discussion focuses on global systems at operational centers. Examples in section 4.1 are drawn from systems at the European Centre for Medium Range Weather Forecasts (ECMWF) and the US National Centers for Environmental Prediction (NCEP).

Meteorological analysis rely on data assimilation, a set of statistical techniques developed to make best use of a wide variety of observations that are irregular in time and space (see, e.g., Kalnay, 2003). Data assimilation optimally combines short-range forecasts with new observations to produce an estimate of the state of the atmosphere at a given time (or the evolution of the atmosphere through the assimilation window). The skill of an analysis therefore depends on the forecast model, the assimilation system, and the available observations. The first two are discussed below; observations relevant to estimates of lower tropospheric water vapor are described in Section 3.

2.1.1 Global forecast models

Data assimilation uses a forecast model to propagate the atmospheric state in time and provide consistency between variables. Practical constraints, including a requirement to deliver timely forecasts, mean that model accuracy must be balanced against computational cost. This impacts model spatial resolution and so the maximum time step. At this writing operational models using equivalent grid spacing[1] of 10 to 20

[1] Grid-point spacing is often equated with resolution but it is well known that, for numerical reasons, the true resolution is less. For instance, from a spectral analysis of ocean winds, Abdalla et al (2013) conclude that in the ECMWF model, 50% of the real variability is only achieved at scales of 3 to 5 times the grid point resolution.

km, time steps of around 10 minutes, and 50-150 levels in the vertical, with the highest between 0.2 and 0.01 hPa. The density of vertical levels is highest near the surface and decreases gradually with height. The vertical discretization especially is relevant to estimates of boundary layer humidity: at typical boundary layer inversion heights the vertical level spacing varies from 200 to 400 m, so that sharp inversions can not be precisely located in the vertical.

Models must also include parameterizations for processes that are not explicitly resolved. In global NWP models the list of parameterized processes might include radiation, shallow and deep convection, cloud macro- and micro-physics, boundary layer turbulence, the impacts of sub-grid orography and gravity waves, and the evolution of the land surface. Despite substantial progress physical parameterizations remain a primary source of model error.

Model errors, whether arising from discretization, numerics, or parameterization deficiencies, impact the quality of the analysis both directly and indirectly, by reducing the effectiveness of observations. Model errors have a larger impact on fields that are only indirectly constrained by observations: e.g. moisture, cloud fields, precipitation and radiative/turbulent fluxes. Parameterization errors are of particular concern in the analysis of water vapor because the field is strongly impacted by heavily-parameterized moist physics.

2.1.2 Data assimilation systems

Data assimilation uses observations to update the state of the atmosphere provided by a short-range forecast. Operational methods rely on the Kalman filter (Kalman, 1960; Kalman and Bucy, 1961) which minimizes the scaled root-mean-square difference between forecasts and all available observations while respecting the uncertainty in both. Covariances propagate information between variables and through space and time so that, for example, an observation of temperature at a given location location can affect temperature, pressure, and winds in the surrounding region. The model-observation difference is computed in the space of the observations so that many observations types, especially the satellite observations described in the next section, rely on forward operators to map the model state to a synthetic (predicted) observation.

Analyses and forecasts are normally paired, with an analysis used to initialize a short (6 to 12 hour) forecast that forms the background field or initial guess for the next analysis. This means that a given analysis is affected by not only the most recent observations but by all observations in the recent past. As a result, in most modern systems the background forecast, which has the history of all previous observations, contains more information about the current state of the atmosphere than do the latest observations, and the difference between forecasts and the resulting analyses is subtle.

Because they rely on forecast models, analyses from continuous forecast/data assimilation cycling provide a self-consistent representation of the atmosphere in space and time. This is convenient; it is also normally more accurate than, for example, estimates for a single observing platform because the analysis exploits many different

data sources (e.g. SYNOP stations, ships and buoys, radiosondes, aircraft, and satellite observations including the passive infrared and microwave and radio occultation described in section 3). The impact of each observation on model state propagates in space and time via the forecasts, leading to better initial estimates of atmospheric state and an improved ability to use the observations (Eyre et al, 1993).

The Kalman filter on which analyses are based is optimal when errors are Gaussian, unbiased, and uncorrelated. All these conditions are violated to some extent in real systems, with detrimental impacts on the analysis. Operational centers typically apply variational bias correction (Dee and Uppala, 2009) to observations, especially those from satellite instruments, to ensure that the observations are unbiased with respect to the model, but this approach cannot distinguish between (possibly conditional) errors in the underlying observations, the forecast model, and the forward operator used to make model state to synthetic observations. Mischaracterization of observation and/or forecast errors can also degrade the analysis, as will be evident in section 5.

2.1.3 Challenges in assimilating moisture

The assimilation of moisture poses special challenges because upper and lower bounds on absolute humidity mean that errors are often unlikely to be Gaussian. This is normally treated by representing humidity in the analysis generation with a specialized control variable that is more likely to be Gaussian: relative humidity, the logarithm of specific humidity, or variance scaled relative humidity (Hólm et al, 2002).

Systematic imbalances between observations and forecast models have historically been an issue for moisture. The ECMWF 40-year Re-analysis (ERA-40; Uppala et al, 2005) reanalysis, for example, contains small systematic positive increments of total column water vapor. This was due partly due to sampling bias in the observations, which were considered only in cloud-free areas, but also reflected errors in the forecast model and the forward operator as well as biases in the observations. Whatever the mix of causes, the model could not retain the excess moisture and precipitated heavily in the initial 12 hours of each forecast, leading to an over-active hydrological cycle and a too-strong Hadley circulation. In more recent systems, which include variational bias correction and make greater use of satellite radiances in cloudy and precipitating areas (Bauer et al, 2010; Geer et al, 2010), the problem is less acute.

Humidity observations over remote tropical oceans consist almost entirely of satellite data (Andersson et al, 2005) from platforms such as those described in Section 3. The observational constraint on total column water vapor provided by passive microwave information is fairly accurate but the broad vertical weighting functions for passive sensors (see Figure 1) mean that the vertical distribution of water vapor in the atmosphere is poorly constrained by observations. As a result the vertical distribution is very much controlled by the assimilating model. In the sub-tropics and stratocumulus areas with subsiding motion, an inversion is maintained as a balance between subsidence and boundary layer entrainment, both of which are controlled primarily by the model formulation (see section 4.1.1).

Table 1 Global re-analyses covering the satellite epoch

Name	Epoch	Reference
ERA-Interim	1979-present	Dee et al (2011)
JRA-55 and variants	1958-present	Kobayashi et al (2015)
MERRA-2	1980-present	`http://gmao.gsfc.nasa.gov/pubs/tm/docs/Bosilovich803.pdf`
NCEP/DOE Reanalysis II	1979-near present	Kanamitsu et al (2002)

2.2 Analysis and reanalysis

In operational NWP centers all components of the analysis system including the forecast model, data assimilation system, and data handling (quality control and bias correction), are improved as opportunities present themselves. This sometimes results in systematic changes in analyzed fields. Reanalysis is the process of analyzing historic observations with a consistent system, normally one which has been improved since the initial analysis was produced. This removes the analysis system as a source of potential discontinuities in analyzed fields although changes in the kind, volume, accuracy, and spatial distribution of available observations can still introduce shifts.

Reanlysis inherits from operational analyses the optimal use of a wide range of observations and the convenience of a gridded, complete, self-consistent description of the atmosphere. There are several key limitations, however. Crucially for some applications is that there is no constraint that energy or mass in a reanalysis be conserved. More generally, estimates of quantities not directly constrained by observations, including the vertical distribution of water vapor over remote oceans, as well clouds, precipitation, and fluxes at the top and bottom of the atmosphere, are less certain and can only be assessed through careful evaluation (Trenberth et al, 2011). This issue is particularly relevant to estimates of water vapor in the oceanic boundary layer, as we show below.

An excellent resource for reanalysis is `https://reanalyses.org`. Some well-known recent global re-analysis projects are listed in Table 1. This list is likely to be out-of-date relatively quickly: ECMWF, for example, has already begun production of the fifth-generation reanalysis ERA5 (`https://www.ecmwf.int/en/newsletter/147/news/era5-reanalysis-production`).

3 What measurements inform current estimates?

Meteorological analyses, as described in 2, rely on observations to correct forecast errors and produce a more accurate estimate of the state of the atmosphere. *In situ* measurements such as radiosondes anchor the observational network but are few and far between over remote low-latitude oceans. Estimates of water vapor in this region rely primarily on three sources of information: sounding instruments that probe the vertical structure of water vapor using the spectral variation of emission by water vapor in the microwave and infrared regions, passive microwave measurements sensitive to column-integrated water vapor, and observations of radio occultation in limb geometry that resolve the density (temperature and humidity) structure with very high vertical resolution but coarse horizontal resolution.

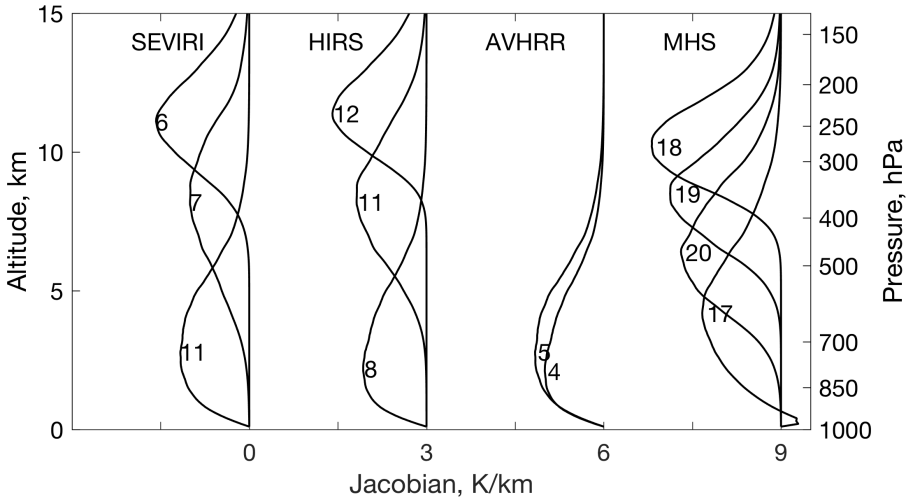

Fig. 1 Water vapor Jacobians for the SEVIRI (a), HIRS (b), and AVHRR (c) infrared and MHS (d) microwave instruments, calculated with the atmospheric radiative transfer simulator ARTS (Eriksson et al, 2011) for a tropical atmosphere (mean of radiosonde profiles for station Manus at 2.06°S, 147.42°E). Curves are labeled with the channel number for the respective instrument. The Jacobian is the derivative of the measurement with respect to changes in the atmospheric state; the figure shows brightness temperature change for nadir-viewing observations resulting from a fractional change in the water vapor concentration, normalized by the layer thickness. Jacobians identify the portion of the atmosphere to which the measurement is sensitive to changes in water vapor and are closely related to weighting functions.

3.1 Microwave and infrared sounding

3.1.1 Principles of measurement

Measurements from microwave and infrared satellite sounders dominate the observations informing water vapor in meteorological analyses (see, e.g., Figure 10 in Dee et al, 2011), especially over remote oceans. These instruments observe radiation emitted by the atmosphere which originates near the altitude where optical depth, the integral of the absorption coefficient calculated from the satellite towards the atmosphere, reaches unity. Sounders exploit two facts. First, clear-sky atmospheric absorption in the troposphere is dominated by water vapor, so that additional moisture makes the atmosphere more opaque and shifts the emission level upward, to colder temperatures, reducing the measured radiance (see for example Buehler et al, 2004, Figure 11). Second, absorption and emission by water vapor depends strongly on frequency, so that measurements made at a range of frequencies with different amounts of absorption are sensitive to the moisture in different atmospheric layers and provide the ability to measure water vapor at different altitudes. This range of altitudes is illustrated by Figure 1, which shows water vapor Jacobians for some widely-used sensors (SEVIRI, HIRS, AVHRR, and MHS, summarized in Table 2). Each of these instruments has flown on multiple platforms; similar "one-off" instruments, such as the SAPHIR instrument aboard the Megha-Tropiques satellite (Brogniez et al, 2013), provide closely-related information.

Table 2 Four widely-used infrared and microwave humidity sensors. IR signifies infrared and MW microwave; GEO denotes geostationary and LEO for low earth (polar) orbit; Δt and Δx approximately specify the temporal and spatial resolution, respectively.

Acronym	Spectral range	Orbit	Δt	Δx	Full name and reference
SEVIRI	IR	GEO	15 min	3 km	Spinning Enhanced Visible and Infrared Imager (Schmetz et al, 2002)
HIRS	IR	LEO	12 h	10 km	High-resolution Infrared Radiation Sounder (Klaes et al, 2007)
AVHRR	IR	LEO	12 h	1 km	Advanced Very-High-Resolution Radiometer (Klaes et al, 2007)
MHS	MW	LEO	12 h	16 km	Microwave Humidity Sounder (Klaes et al, 2007)

Passive satellite sounding with infrared imagers has a long history. Readily available infrared humidity data start with the HIRS instrument on the TIROS N satellite in 1978 (Shi and Bates, 2011). Meteorological microwave satellite measurements also have a long history, but water vapor profile measurements (near 183 GHz) only became available with the SSM/T2 instrument on the DMSP F11 satellite in 1991, with data in the NOAA CLASS archive starting in 1994.

Legacy instruments have just a few (one to five) channels dedicated to water vapor; this provides a strict upper bound on the number of degrees of freedom in the vertical profile of water vapor that can be resolved. The strength of these sensors lies in their horizontal resolution (1-15 km , see Table 2) and the resulting ability to resolve horizontal structures.

Figure 2 highlights the kind of information available from microwave and infrared sounding instruments. Here the image comes from channel 11 of the SEVERI instrument, which is sensitive to water vapor below about 6 km (Fig. 1). The measurement is expressed as a brightness temperature T_b i.e. the temperature at which a black body would produce the observed channel-integrated intensity. For SEVERI and similar instruments (downward-looking viewing geometry, in optically-thick frequency regions dominated by water vapor absorption) T_b can be easily interpreted: because the thermal source function for the radiative transfer (the Planck function) depends on temperature, while the atmospheric absorption depends on the water vapor content which is itself also strongly controlled by the temperature, the measured intensity is a good proxy for relative humidity averaged over the layer. High T_b indicate emission from lower in the layer, and hence low relative humidity.

These relationships may be used to develop scalings between observed T_b and layer-averaged relative humidity (e.g. Buehler and John, 2005); in this image a 1 K change in T_b corresponds to approximately 9% relative difference in relative humidity. In practice, however, data assimilation systems use radiative transfer calculation using fast models (also called "forward operators") to predict the intensity that would be observed for a given distribution of temperature and humidity, and the data assimilation system works to minimize the difference between these predicted observations and the observations themselves (see section 2.1.2).

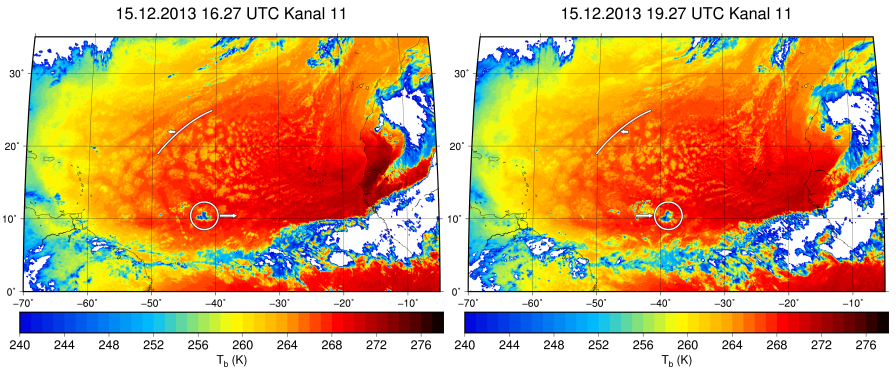

Fig. 2 Two different snapshots of water vapor brightness temperatures by SEVIRI Channel 11, separated by 3 h. The line indicates humidity and cloud structures below roughly 6 km, moving westward; the circle indicates an overlying high cold cloud, moving eastward. These images were taken in December 2013 over the tropical Atlantic. Brightness temperatures below the (somewhat arbitrary) threshold of 240 K are shown in white to indicate deep convection.

3.1.2 Why both microwave and infrared observations are useful

Figure 2 was obtained from an infrared sounder on a geostationary satellite; instruments on such platforms can provide very high time resolution observations (15 m or less). It is not practical to deploy microwave sounders so far from the Earth because their spatial resolution would be greatly compromised. Spatial resolution is limited by diffraction, thus infrared sensors inherently allow higher spatial resolutions than microwave sensors, because their apertures are much larger compared to the measured wavelength.

But the figure also illustrates why microwave sounders provide such a useful complement to infrared observations. Brightness temperatures T_b below some threshold, as occur frequently in the image, correspond to relative humidity above saturation. This unphysical result indicates the presence of clouds. It is relatively easy to filter out the cloud contaminated data, but restricting humidity observations to clear skies along can lead to biases in average humidity and even its climatic trend (John et al, 2011). Microwave sensors are much less affected by clouds, and so continue to be central to meteorological analyses despite the relatively low horizontal resolution.

3.1.3 Prospects

The Jacobians of passive sensors are broad in the vertical (Fig. 1) because the radiation received at the sensor arises from a range of altitudes. Hyperspectral infrared instruments, including AIRS (Aumann et al, 2003) with 2378 channels and IASI (Clerbaux et al, 2009) with 8461 channels, offer the possibility of combining many high-accuracy channels to achieve higher vertical resolution, analogous to the sharpening of a blurred image in image processing (see for example Osher et al, 2005). (Hyperspectral microwave sensors do not yet exist but may be feasible in a few years, as discussed in the contribution by Nehrir et al. to this volume.)

The true information content from hyperspectral observations, however, is orders of magnitude lower than the number of channels because the measurements in individual channels are very highly correlated. Applying the Bayesian information content analysis described in more detail in Nehrir et al. to IASI, for example, shows that at most 16 independent pieces of information on the water vapor profile are theoretically possible, corresponding to a vertical resolution of approximately 1.5 km in the troposphere. In practice the information content of IASI is lower, with literature estimates ranging from 3 to 10 pieces of independent information (August et al, 2012; Herbin et al, 2009; Lacour et al, 2012; Schneider and Hase, 2011). This may be firstly because often only a small subset of the channels is used, and secondly because in an NWP context better a priori information is available, which reduces the information content of the measurement relative to the a priori.

Ultimately, it is the physics of radiative transfer that limits the ability of passive sensors to probe the humidity structure of the lower troposphere.

3.2 Estimates of precipitable water from microwave observations

Constraints on total column water vapor come from observations in spectral regions where atmospheric absorption is weak enough that the surface is visible from space. This works particularly well in the microwave spectral region over ocean, because there the surface is radiatively cold and can be accurately modeled (the emissivity is around 0.6 and depends mostly on the wind speed). The atmosphere is then observed in emission in front of the cold background, and Jacobians are positive, instead of negative as in Figure 1. The temperature dependence of the Planck function and the temperature control of absolute humidity then combine to make the measurement depend strongly on the total column water vapor.

Mears et al (2015) validated such satellite-borne microwave total column water vapor measurements against ground-based GPS observations and found an overall bias of only approximately $1\,\mathrm{kg/m^2}$ and standard deviations better than approximately $2\,\mathrm{kg/m^2}$.

3.3 GNSS radio occultation – a global refractometer

An orthogonal source of water vapor information comes from observations of Global Navigation Satellite System (GNSS) radio occultation (RO) using the refraction of decimeter-wave GNSS signals near 1.2 GHz and 1.6 GHz received at low Earth orbit (LEO) satellites.

3.3.1 Principles of measurement

Figure 3a illustrates the GNSS RO observing geometry and summarizes the steps in estimating profiles of atmospheric state from phase measurements (see also Anthes, 2011; Kursinski et al, 1997; Steiner et al, 2011). An occultation event occurs when a receiver, peering through the atmosphere towards a satellite with a GNSS transmitter in limb sounding geometry, observes the satellite setting behind or rising above

the Earth's horizon. Profiles are assigned a horizontal position at point of closest approach to the Earth's surface ('tangent point') although the information derives from an along-path range of roughly 100 km to 200 km around the tangent point in the troposphere with across-ray resolution of 1-2 km.

The fundamental measurement is of time delays of GNSS signals during occultation events, which can be directly related to excess phase paths. Because the measurement is based on time, which is uniquely well measured, RO measurements have unique long-term stability and narrow uncertainty. GNSS signals are not attenuated by clouds, so that sampling is unbiased. The vertical resolution of RO measurements, roughly 200-300 m (Gorbunov et al, 2004; Kursinski et al, 1997), is much higher than passive microwave and infrared sensors (Sec. 3.1). The primary disadvantage is that data are relatively sparse. The only system exploited to date for GNSS RO measurements is the U.S. Global Positioning System (GPS); with this constellation a single RO receiver in LEO acquires 300 to 600 RO events per day with global coverage.

Interpretation of RO refraction measurements is quite different than for brightness temperatures. Tracking and orbit data are used to compute excess phase profiles (Anthes, 2011; Hajj et al, 2002; Schreiner et al, 2009) which are converted to Doppler shift profiles and then bending angle profiles (Ho et al, 2012; Steiner et al, 2013, and references therein). Bending angle profiles may be used in data assimilation or may form the basis of retrievals. The latter map bending angle to refractivity and dry-air profiles and finally to thermodynamic profiles of density, pressure, temperature, and tropospheric water vapor (Kursinski and Gebhardt, 2014; Li et al, 2016) .

3.3.2 Vertical resolution, accuracy, and limitations

Although meteorological analyses incorporate RO observations using their own forward operators (e.g. Healy and Thepaut, 2006) the accuracy of the underlying observations is more clearly demonstrated by comparing retrievals of temperature and humidity to *in situ* observations, as in Figure 4. Here the comparison is to Vaisala RS92 radiosonde profiles from the Global Reference Upper Air Network (GRUAN), which undertakes dedicated efforts to provide climate-quality processing of the data (Bodeker et al, 2016; Immler et al, 2010). Panels a and b show example profiles containing layered moisture structures (see also Stevens et al, 2017), illustrating the high vertical resolution. The reference radiosonde profiles (GRUAN RS92-GDP.2) are used at $\sim$300 m vertical resolution, while the RO profiles, taken from the recent OPSv5.6 re-processing of all 2001-2016 RO data at the Wegener Center, were not yet optimized for water vapor profiling and so are only available at $\sim$800 m vertical resolution. Profiles from the operational analysis produced at ECMWF are also shown. Even at reduced vertical resolution RO captures moisture layering that is smeared out in the analysis profiles.

Panels c and d shows difference statistics between RO temperature and humidity profiles collocated with GRUAN profiles. Specific humidity is consistent between the two data sets to within 0.1-0.3 g/kg in the median, consistent with theoretical studies of accuracy (e.g. Kursinski and Gebhardt, 2014; Ladstädter et al, 2015; Rieckh et al, 2016). Some amount of disagreement between radiosonde and RO profiles is

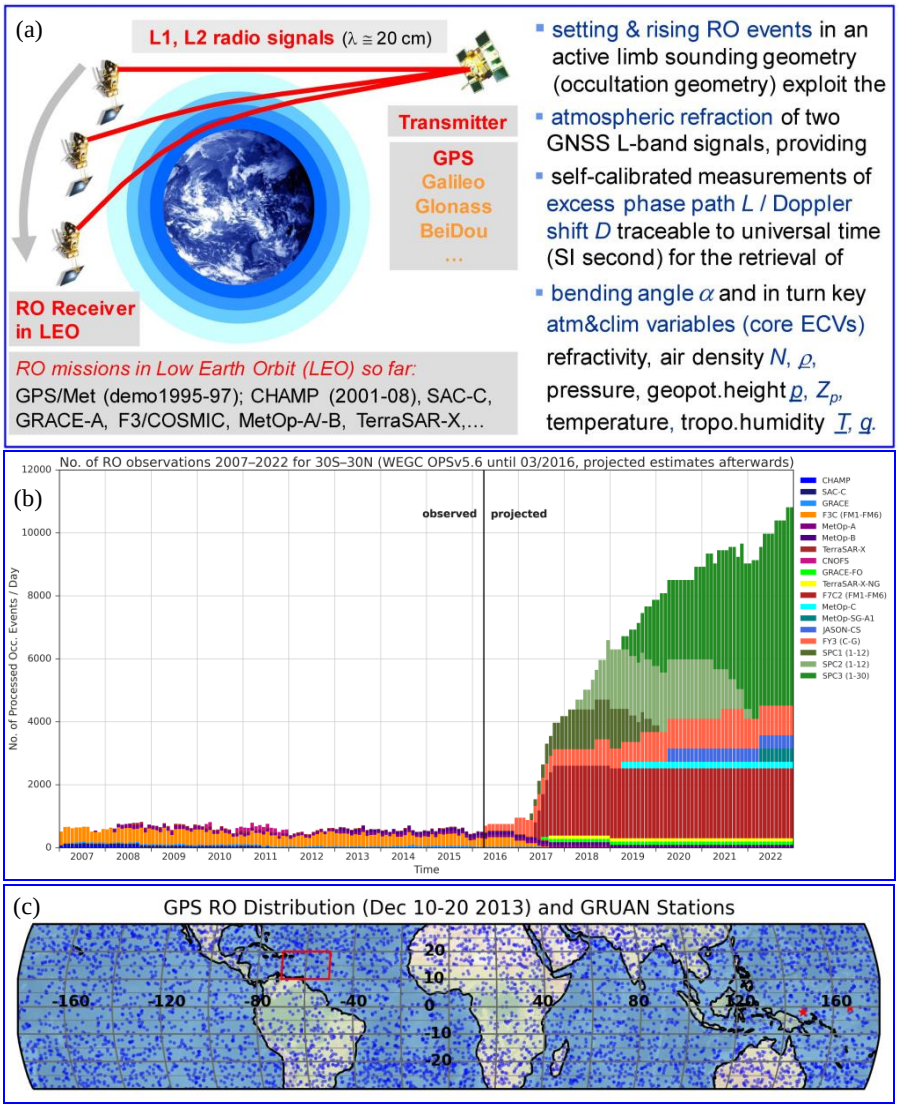

Fig. 3 (a) Schematic view of the GNSS RO active limb sounding observation geometry and explanation of measurement principles, after Kirchengast et al (2016); the acronyms for RO missions are the common names in the RO literature. (b) Number of RO events per day over 2007 to 2022 at low latitudes (30S-30N), with actual numbers until 2016 and with projected numbers afterwards, where new RO missions currently prepared are successively deployed. (c) Coverage by RO events (blue dots) at low latitudes (30S-30N) during 10-20 December 2013 (NARVAL- South campaign), with showing a zoom also for a cell in the Barbados area (red box). Two available tropical GRUAN radiosonde stations are marked (red asterisk symbols)

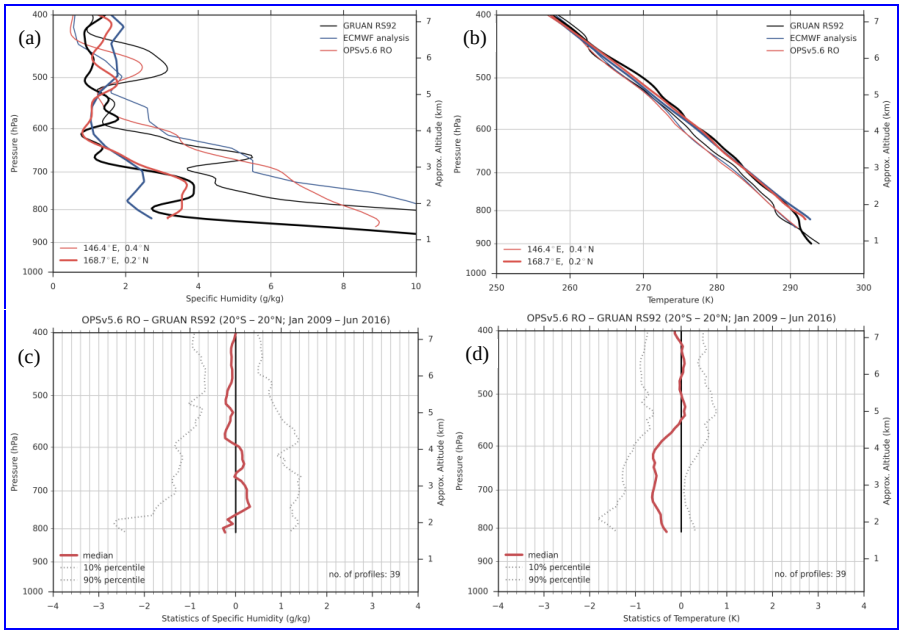

Fig. 4 Individual examples profiles of specific humidity (a) and temperature (b) from inter-comparing RO and ECMWF to collocated GRUAN data (about 200 km-2 hr space-time difference in the two cases). Furthermore, statistics (median deviation and indicative percentiles) of RO specific humidity (c) and temperature (d) profiles are shown relative to GRUAN data, based on the available 300 km'3 hr collocations over 2009-2016. The tropical GRUAN stations available are those marked in Fig. 4c.

expected due to imperfect collocation – sparse sampling by RO requires the use of relatively loose criteria for co-location ($\pm$300 km, $\pm$ 3 h) to obtain enough samples.

Figure 4 also illustrates an important limitation of RO observations: information is available through the free troposphere, including the very valuable RO capacity of determining the boundary layer height (e.g. Anthes, 2011; Ho et al, 2015), but is lacking within the atmospheric boundary layer. The retrieved RO profiles in Fig. 4a,b stop near the boundary layer top, which in one case is clearly indicated by the GRUAN profile. Though efforts are being made to exploit RO observations to determine boundary later water vapor (e.g. Sokolovskiy et al, 2014; Xie et al, 2012), the core strength of existing RO observations is in profiling of the free troposphere.

3.3.3 Prospects

Radio occultation measurements provide a valuable complement to observations by passive microwave and infrared sensors (Sec. 3.1) for characterizing water vapor. The observations play an important role in data assimilation systems (Sec. 2) because the high accuracy, itself a result of the ability to make the fundamental measurement of time with high accuracy, means that they can be incorporated as 'anchor observations' without bias correction, adding a globally-distributed set of calibration points to the radiosonde network. When the measurements are used outside assimilation systems

they are able to accurately determine the height of the boundary layer; this capability might be especially useful in process studies.

The record is short compared to passive imagers: limited data is available from 2001 with the full existing system online only since 2007. Data are also relatively sparse horizontally. This sparsity means that RO observations are often more useful over the long term, say via their incorporation into (re-)analyses, then for limited-domain field campaigns. This is evident in Figure 3c, which shows all low-latitude RO event locations during the NARVAL-South campaign between 10 and 20 December 2013 (Stevens et al, 2016). This field campaign focused on the region around Barbados (red 10° x 20° box). The entire low latitude band received 5759 RO events during this 11-day period; just 67 events occurred in the Barbados area.

The amount of GNSS data is posed to increase rapidly, however. Initial results have been obtained from the Chinese BeiDou system (Liao et al, 2016) and use of the European Galileo and Russian Glonass systems is expected in the next years. This will vastly expand the frequency of RO events. Figure 3b illustrates the total numbers available over the last decade at low latitudes within 30°S to 30°N, around 600 events per day, and the projected strong increase by about an order of magnitude over the coming years. This leads to more than 8000 events per day as of 2020, which corresponds to more than 20000 events per day globally.

Current observations rely on GNSS radio occultation. One promising technological advance is LEO-LEO occultation (Kirchengast and Schweitzer, 2011; Kursinski et al, 2002; Liu et al, 2017), described as one of the emerging water vapor observation techniques by Nehrir et al. in this issue.

4 Errors in water vapor distributions and the resulting impacts

Satellite observations (section 3) are used in analysis systems (section 2) to produce estimates of the state of the atmosphere including the distribution of water vapor. The accuracy of this estimate over remote oceans, especially in the lower troposphere, has implications for the ability to use observations to test and generate hypotheses. In this section we use observations to spot-check this distribution in two circumstances.

4.1 Assessing errors in the analyzed distribution of water vapor

Because analyses are constructed by minimizing the difference between the state and all available observations, the accuracy of an analysis can be assessed only by comparison with independent observations. This is harder than it might seem – to produce the best possible analysis, forecasting centers go to great lengths to use all available high-quality observations, going so far as to facilitate the real-time availability of data from field campaigns. This means that opportunities to assess specific aspects of analysis, such as lower tropospheric water vapor over low-latitude oceans, are few and far between.

Below we exploit two sets of radiosonde measurements made during field campaigns to assess the accuracy of water vapor analysis. Section 4.1.1 compares radiosonde observations off the coast of Peru to fields in the ERA Interim reanalysis,

which did not assimilate these observations. Section 4.1.2 exploits measurements made in the equatorial Pacific to assess a reduced-resolution version of the current NCEP data assimilation using data-denial experiments in which the observations were deliberately withheld. Both reanalyses make use of the full range of satellite observations as described in section 3; the precise observations used will vary from day to day. Because the comparisons involve different analysis systems from different epochs, assessed in very different meteorological regimes, we do not expect the errors identified here to be consistent with each other, or representative in any broad sense. Our intent is rather to highlight similarities in the character and magnitude of errors and, in the next section, to ask to what extent these might be ameliorated with better observations of lower tropospheric water vapor.

4.1.1 Assessment in subsiding regions

The first example comes from radiosondes launched as part of the EPIC (Eastern Pacific Investigation of Climate Processes in the Coupled Ocean-Atmosphere System) campaign. This experiment took place from 16-21 October 2001 at 20°S/85°W in the East Pacific, a little over 800 km off the coast of Peru and Chile (Bretherton et al, 2004). We use 3-hourly radiosondes launched from the research vessel Ron Brown to assess the widely-used ERA Interim reanalysis (ERA-I; Dee et al, 2011). The comparison exposes analysis error because the soundings were not used in the reanalysis.

In the EPIC domain subsidence and relatively cold sea-surface temperatures frequently give rise to stratocumulus clouds under strong thermal and moisture inversions. These clouds are notoriously difficult to simulate in global models, partly because the inversions are very sharp and so poorly resolved on a relatively coarse numerical grid. Like much of the low-latitude oceans, few *in situ* observations were available for assimilation, so it is of interest to see how an analysis system copes.

Figure 5a shows the profile of specific humidity averaged over the entire period. A sharp jump in specific humidity is observed at the top of the boundary layer. ERA-I reproduces an inversion but it is too low (at 1147 m and 918 m, by about one model level) and not sharp enough. The profile of potential temperature (not shown) indicates a consistent picture. There are no observations in ERA-I that impose sharp temperature and moisture gradients. Instead, the inversion is maintained by the model as the result of a subtle balance between weak subsidence and the entrainment process in the model physics.

The evolution of moisture in the observations and the reanalysis is illustrated in time-height cross section in Fig. 6. The mixed layer is more moist than observed. This is tied quite closely to the overly-shallow boundary layer: since total column water vapor is well constrained by satellite microwave observations, the too-low inversion is compensated by excess boundary layer moisture. Temporal variability is also more muted in the analysis than in the observations, although the diurnal cycle is more regular than is observed. The observed variability includes a component of sampling or representativeness noise, but much of the observed variability is coherent over a period of 3 hours, suggesting that the reanalysis does indeed miss some amount of variability. Finally, a moist layer descends from 4000 m on 16 Oct to about 2000 m on 20 Oct. Such a structure is related to the large scale flow and ERA-I seems to

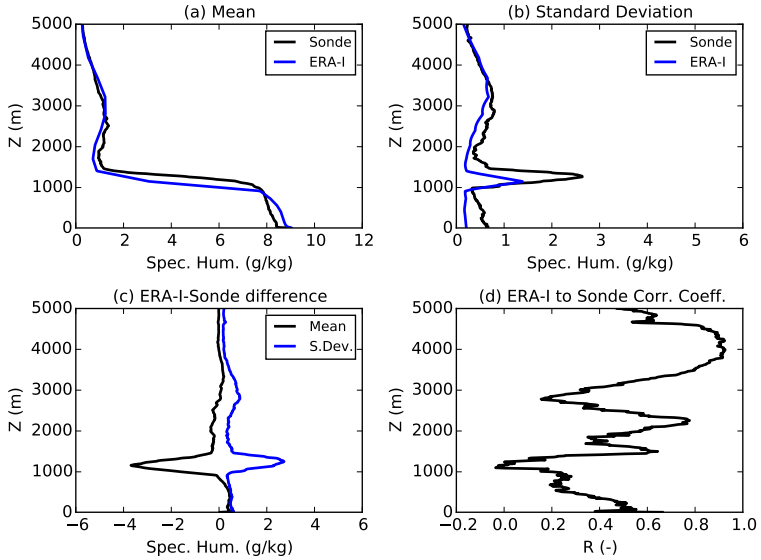

Fig. 5 (a) Mean radiosonde and ERA-I humidity profiles, (b) Standard Deviation of sonde and ERA-I humidity profiles, indicating temporal variability, (c) Mean and standard deviation of difference in humidity between ERA-I and sonde, and (d) correlation coefficient of humidity between ERA-I and sonde.

capture the large scales of this feature rather well, but the smaller scale variability is smeared out.

The statistics of the variability are summarized in Fig. 5b,c,d. The correlation between ERA-I moisture and sonde observations varies strongly with height. The relatively low correlation between observations and analysis is due to the narrow range of conditions experienced at this single point, lack of variability in the forecast model (evident in panel b), and representativeness noise in the observations. The correlation drops to zero at a height of 1000 m, but this is due to the mismatch in inversion height: the 1000 m level is above the inversion in ERA-I and just below the inversion in the observations, so the time series are uncorrelated.

4.1.2 Assessment in convecting regions

A second opportunity for assessment, this one focused on regions of deeper convection, arises from a NOAA field campaign aimed at studying deep convection associated with sea surface temperature anomalies. The El Niño Rapid Response field program (ENRR, see `https://www.esrl.noaa.gov/psd/enso/rapid_response/`) included dropsondes from the G4 aircraft and radiosonde launches from the island station at Kiribati and the research vessel Ron Brown, which was moving. Here we explore the impact of these sondes in a global assimilation with the currently-operational NCEP hybrid ensemble-variational data assimilation system (Kleist and Ide, 2015; Wang et al, 2013) using 80 members. The assimilation is similar to oper-

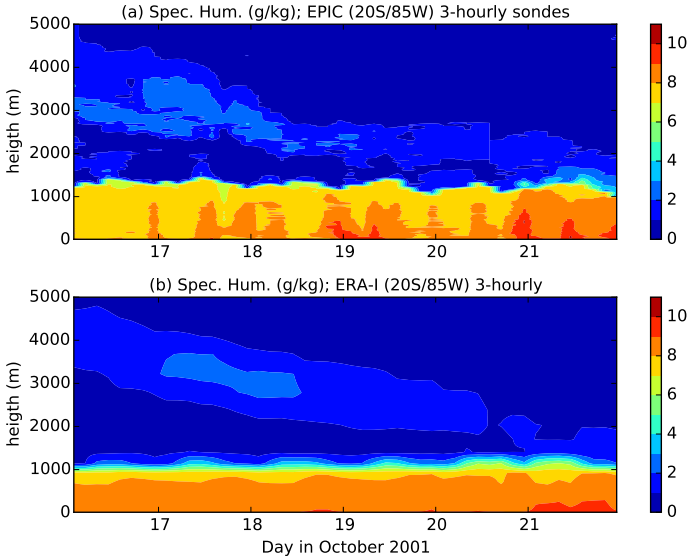

Fig. 6 Time height cross section of 3-hourly radio sonde observations of specific humidity (top panel) and 3-hourly ERA-I reanalysis data. The time axis covers the EPIC campaign from 11 to 16 Oct 2001 at the "stratus buoy" location in the Eastern Pacific (20°S/85°W).

ational analyses in using all available observations including conventional observations, GPS radio occultation, satellite radiances, etc. but is run at reduced horizontal resolution (T254).

We assess the representation of lower-tropospheric water vapor by using "data denial" experiments in which the ENRR soundings were evaluated (i.e. the error between forecast and observations was computed) but did not affect the analyzed state. (A parallel set of assimilations in which the sondes did contribute to the analysis is used in Section 5.1). The forecast/assimilation system was cycled through all of February and March 2016. The original observations have quite high vertical resolution (c.f. Stevens et al, 2017) but were introduced into the analysis system, and are examined here, at a greatly reduced vertical resolution to prevent over-fitting. We restrict our attention to observations made west of 139°W, which excludes a leg of soundings made by the ship much closer to the western coast of North America.

Figure 7, the analog to Fig. 5, provides an overview of water vapor as observed (in blue) and in the analysis (red). Here all soundings are considered independently although many more dropsondes were launched from the G4 (529) than from Kiribati (54) or from the Ron Brown (69). The domain is deeper than in Fig. 5, extending to 250 hPa or roughly 10.5 km. No sharp inversion is evident in the mean sounding, partly as a result of sampling a much wider range conditions and partly because weaker subsidence in this region leads a wider variety of convection. Variability in specific humidity is largest in the layer between roughly 800 and 600 hPa reflecting variability in shallow and congestus convection; this variability is roughly captured,

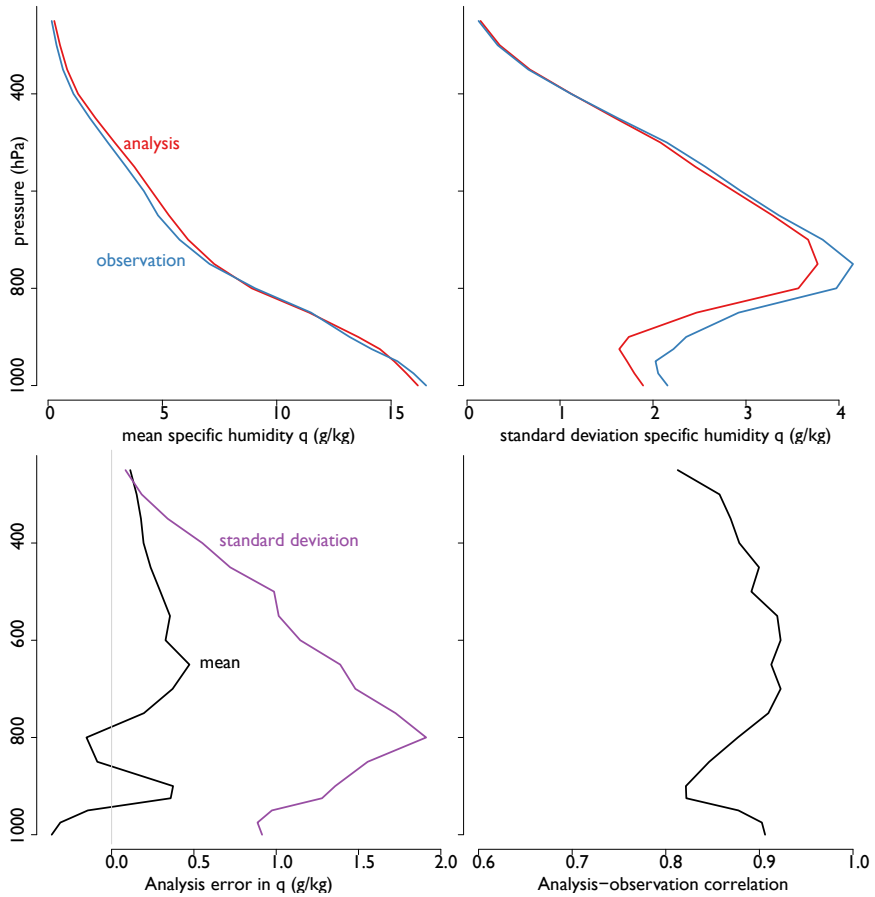

Fig. 7 As in Fig. 5 but for observations in the Tropical Pacific obtained during the El Niño Rapid Response Campaign. Observations include dropsondes from an aircraft and radiosondes launched at an island station and by a ship traversing the domain. Assimilation uses a reduced-resolution version of the operational system at the US National Centers for Environmental Prediction. (a) Mean sonde and analyzed specific humidity profiles, (b) Standard deviation of sonde and analyzed specific humidity profiles, indicating temporal and spatial variability, (c) Mean and standard deviation of difference in humidity between analysis and observations, and (d) correlation coefficient of humidity between analysis and observations.

if at somewhat reduced amplitude, in the analysis (upper right). The analysis is too dry in the boundary layer and too moist in the free troposphere, with modest values in absolute terms (less than 0.5 g/kg) that become large when expressed as relative humidity at lower pressures. The relatively high correlation between analysis and observations (lower right) indicates that the analysis is able to reproduce regional and synoptic variations reasonable well.

In practice the three platforms from which soundings are available sampled somewhat different environments (Figure 8). Soundings from the fixed station at Kiritimati Island in the Republic of Kiribati, just off the equator, are systematically wetter and

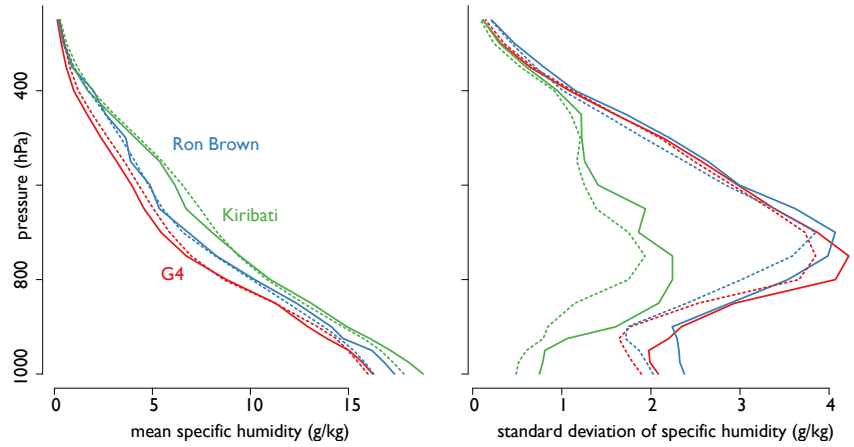

Fig. 8 Mean (left) and standard deviation of specific humidity in the El Niño Rapid Response soundings available from the G4 dropsondes (red) and from radiosondes launched from the Ron Brown (blue) and from Kiritimati Island in Kiribati (green). Solid lines show the observations and dashed lines the colocated analyses in experiments neglecting the sondes. Soundings from Kiribati, near the Equator, are systematically warmer and wetter than those obtained from the traveling platforms. The analysis captures the overall differences in the sampling of the large-scale environment but under-represents the variability.

less variable than soundings from the ship and aircraft, which sampled a much wider range of geographic locations as far as 20°from the equator. Soundings from the Ron Brown are systematically moister than from the G4 with the region of maximum variability perhaps 50 hPa higher, suggesting greater sampling of congestus convection; this difference is at least partly the result of the flight paths on the G4 being constructed to avoid hazardous large-scale regions of deep convection.

The analysis captures the broad-brush and synoptic differences among the sources of the soundings. Temporal variability is somewhat smaller in the analysis than in the soundings (compare the dashed and solid lines in Fig. 8, right panel) although some amount of the observed variability arises from sampling noise.

Because errors are relatively small, however, assessments of error can be sensitive to averaging assumptions. Figure 9 shows the analysis bias (left), standard deviation (right, dashed lines) , and root-mean-squared error (right, solid lines) in specific humidity. Estimates from all three platforms suggest that the analysis underestimates humidity in the boundary layer. The moist bias in the free troposphere (Fig. 7), however, is less robust. The bias is positive and largest in magnitude in soundings taken by the G4, which avoided regions of organized deep convection.

This suggests that the contrast in mid-tropospheric water vapor between regions of large-scale deep convection and the surrounding environment may be underestimated. To the extent that large-scale organization is influenced by convective self-aggregation (Wing et al, 2017) this implies that the observed (Tobin et al, 2012) and modeled (e.g. Bretherton et al, 2005) contrast in humidity associated with convective organization may not be fully captured in the analysis.

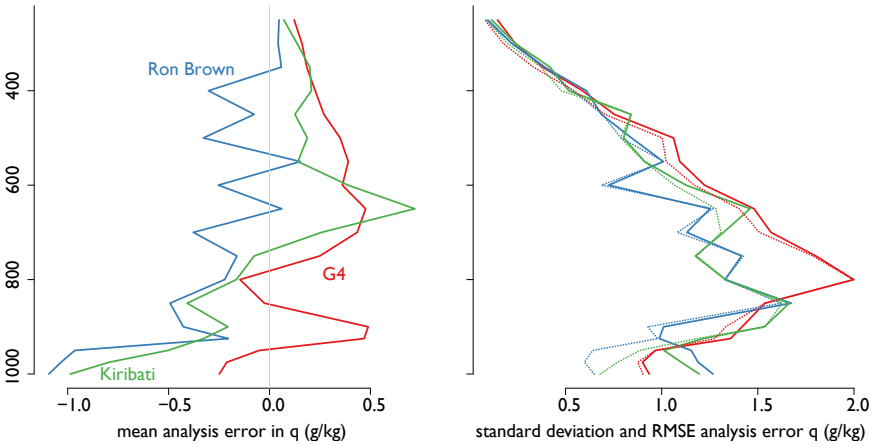

Fig. 9 Bias (analysis minus observations, left), standard deviation (right, dashed lines), root-mean-square error (solid lines) in specific humidity in the El Niño Rapid Response soundings. The G4 soundings, which preferentially sample outside extensive deep convection, also exhibit bias from roughly 700 - 500 hPa, suggesting that analysis underestimates the contrast between large-scale moist and dry regions.

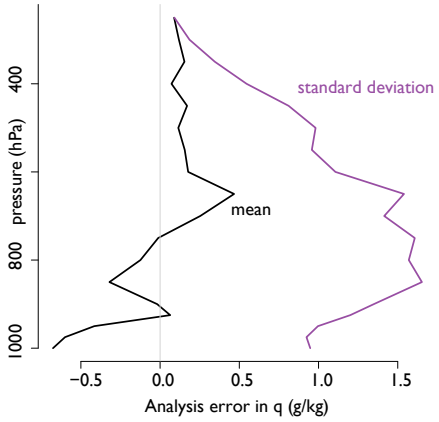

Fig. 10 Mean and standard deviation of difference in humidity between analysis and observations, computed using equal weights for soundings from the G4 and Ron Brown (and hence commensurate weights for all three sets of soundings). This reduces the impact of sampling biases in the G4 soundings on the overall estimate of error. The analysis systematically underestimates boundary layer humidity and overestimates humidity in the free troposphere and may underestimate the depth of the boundary layer.

Soundings from the G4 are far more numerous than from the other sources and so dominate the estimates of analysis error in Fig. 7. Figure 10 repeats the lower left panel of this figure giving equal weight to the G4 and Ron Brown soundings. This more geographically-representative view makes it clear that the analysis systematically underestimates boundary layer humidity and overestimates humidity in the free

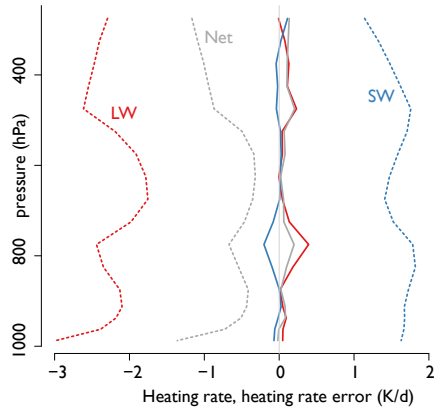

Fig. 11 Errors in longwave (red), shortwave (blue) and net (grey) heating rates arising from analysis errors in temperature and humidity. Dashed lines show mean heating rates.

troposphere. The excursion towards more positive bias at 900 hPa is consistent with the boundary layer being deeper in the analysis than in the observations.

4.2 Assessing impacts

As described in the introduction, the distribution of water vapor in the troposphere is intimately linked to convection and cloudiness because radiative cooling provides the destabilization needed to initiate convection and to determine large-scale vertical motion. Radiative cooling rates throughout the atmosphere are affected by the full vertical distribution of water vapor, so errors in water vapor abundance have non-local and non-obvious impacts on cooling rates. Figure 11 shows the impact of analysis errors in specific humidity on clear-sky radiative cooling rates, computed by applying the SOCRATES radiative transfer model (a heavily-revised version of the code described in Edwards and Slingo, 1996) to the observed and analyzed temperature and humidity fields, then averaging across the heating rate differences. As in Fig. 10, each set of soundings is given roughly equal weight. Present-day concentrations of other well-mixed greenhouse gases are assumed. Water vapor abundance affects longwave (red) and shortwave (blue) fluxes in the opposite sense, i.e. increased humidity leads to more efficient longwave radiative cooling but also increased solar absorption. As a result net clear-sky cooling rates through the atmosphere are 0.5-1 K/d, with mean errors of 0.05-0.1 K/d, or roughly 10%, below 600 hPa, increasing to 0.15 K/d in the upper free troposphere where net cooling also increases.

Analysis errors in the radiative cooling (and resulting subsidence rates) to which low clouds are quite sensitive, especially errors that affect the ability of a re-analysis to identify regional and/or interannual contrast, can compromise observational studies of low cloud feedbacks (Klein et al., this issue).

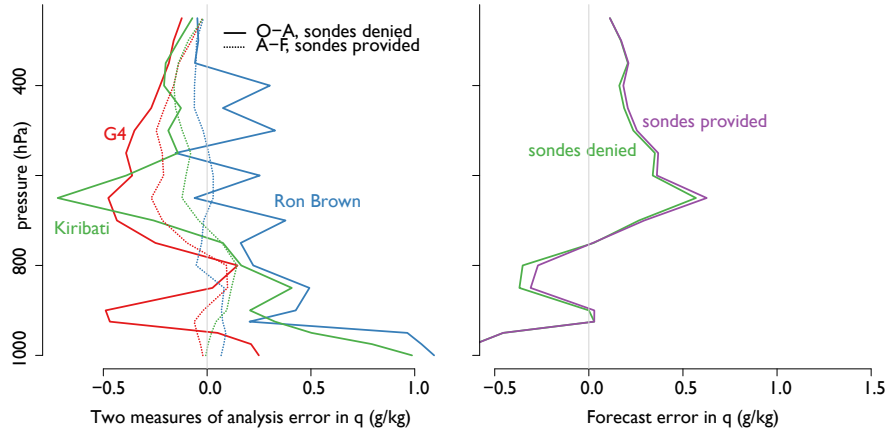

Fig. 12 Left: Two views of systematic analysis error in specific humidity. Solid lines show the mean difference between withheld observations and analysis for each data source. (The same data are shown, with opposite sign, in the left panel of Fig. 9). Dashed lines show the mean analysis increment for specific humidity, i.e. the amount by which the forecast is changed by all observations, in data assimilation experiments in which the soundings are included. Increments are small below 850 hPa even though bias is large there, reflecting both larger observational uncertainty and more certain but erroneous forecasts. Right: Mean forecast error in specific humidity, evaluated against evenly-weighted sets of sondes, in assimilation experiments that include (purple) or neglect (green) the observations. Much of the improvement in the analysis of specific humidity is lost within the 6-hour forecast window, suggesting that analysis quality in humidity is strongly affected by model error.

5 Characterizing water vapor in a more richly observed world

As described in Sec. 3, present-day systems for routinely observing water vapor over remote oceans provide a relatively strong constraint on the vertical integral but a blurred view of the vertical distribution. Analyses of specific humidity that incorporate these loose constraints into imperfect models therefore exhibit errors in the vertical distribution (Figs. 5, 7). In particular, the lack of an observational constraint on boundary-layer humidity allows analysis systems to make compensating errors that preserve column-integrated water vapor. In these very limited comparisons the ERA-Interim system produces a boundary layer roughly 10% too shallow and 10% too moist, while errors in the current NCEP system (too dry in the boundary layer, too moist above) result in an artificially enhanced moisture contrast between the boundary layer and the free troposphere. The analyses do capture the bulk of the large-scale variability, although the NCEP system may underestimate the contrast in humidity between convective and non-convective regions.

Far more sophisticated technologies for the remote sensing of water vapor are emerging, however, (see Nehrir et al., this volume). Might much better observations lead to greatly improved analyses of water vapor?

5.1 Limited observations and model error

Figure 12 explores the impacts of the two most important sources of analysis error, namely model error and a lack of constraining observations, in the NCEP system. The left panel illustrates the impact of observations on the analysis by comparing the bias in specific humidity (solid lines), computed separately for each set of soundings, with the analysis increment in humidity averaged over the same locations in a parallel set of assimilations in which the observations *do* impact the analysis (dashed lines). Increments measure the degree to which all available observations change the short-term forecast; the degree to which increments averaged over time and space are non-zero reflects systematic model errors (Klinker and Sardeshmukh, 1992; Rodwell and Palmer, 2007).

At pressures below roughly 800 hPa the increments track the bias and its variation among sounding sources, indicating that the observations counteract systematic model error. The increments are not as large as the bias because the assimilation strikes a balance between the uncertainties in the observations and in the forecast (measured here by the ensemble spread).

Increments are small, however, at pressures above 800 hPa, where bias in humidity is largest. This partly reflects the fact that observations are thought to be less certain (specifically, less representative of large-scale conditions) closer to the atmosphere-surface interface. But it is also the result of limited variation in humidity across the ensemble in the lower troposphere, driven partly by the fact that all members of the ensemble see the same sea surface temperature field. The result is that forecasts of lower tropospheric humidity are confident, so that low relative weight is assigned to the observations, but are nonetheless in error. The analysis is therefore unable to exploit the detailed information fully, and remains in error despite strong observational constraints from the soundings.

5.2 Exploiting richer observations

Observations that directly characterize boundary layer humidity, such as those obtained from field campaigns or from future observing systems, do improve the analysis of humidity throughout the atmosphere. The impact of the observations is limited, however, due to systematic model errors, lack of model variability, and errors in the background error estimates of global analysis systems. This applies especially to water vapor concentration, which is strongly affected by parametrization of processes with short time scales. Indeed, the observations collected during the El Niño Rapid Response campaign had little impact on even the 6-hour forecasts used as background states in the forecast/assimilation cycles. The right panel of Fig. 12 shows the mean difference between observed and forecast specific humidity in that neglect (green) or include (purple) the equally-weighted sets of sondes. The forecast departures are quite similar in both experiments, indicating that improvements in the humidity analysis brought by the sondes don't last even as long as six hours in the deep tropics.

Analysis systems provide the best currently-available routine view of the distribution of water vapor over remote oceans, capturing much of the large-scale variability

even as the vertical distribution is compromised by model error and observations that provide a relatively loose constraint on humidity near the surface. More detailed observations of the vertical structure of water vapor, especially in the boundary layer, would lead to an improved representation, especially if forecast model and assimilation systems are improved to better exploit the new observations. This will require better characterization of model error, as well as better characterization of error variances/covariances to allow analysis systems to represent vertical structures ranging from sharp inversions of the subtropics to more blended inversion structures of the deep tropics. High resolution observations would, if made routinely, also provide the information needed to identify and correct systematic model errors.

In addition to the vertical structures caused by large scale transport, detailed field observations also show fine scale structures that have the signature of convection (for example as described by Stevens et al (2017) and Kiemle et al., this issue). Such a mesoscale analysis will require both high frequency and high resolution observations as well as new assimilation techniques adapted to structures with a relatively short predictability horizon.

Acknowledgements This paper arises from the International Space Science Institute (ISSI) workshop on Shallow clouds and water vapor, circulation and climate sensitivity. We thank Oleksandr Bobryshev for preparing Figure 1 and deriving scaling parameters and cloud thresholds in Section 3.1,Theresa Lang for preparing Figure 2, and Lukas Kluft and Mareike Burba for IASI performance estimates. We thank the GRUAN project for tropical radiosonde data and M. Schwaerz and WGC's Occultation Processing System team for provision of OPSv5.6 RO data. K. Franklin Evans provided the SOCRATES radiative transfer calculations in Section 4. R.P. was supported by the U.S. National Science Foundation under grant ATM-1138394. Contributions by G.K. and F. L were funded by the Austrian Research Promotion Agency (FFG) under the projects OPSCLIMTRACE-OPSCLIMVALUE and by the Austrian Science Fund (FWF) under the project VERTCLIM (P27724-NBL).

References

Abdalla S, Isaksen L, Janssen P, Wedi N (2013) Effective spectral resolution of ECMWF atmospheric forecast models. ECMWF Newsletter 137:19–22

Andersson E, Bauer P, Beljaars A, Chevallier F, others (2005) Assimilation and modeling of the atmospheric hydrological cycle in the ECMWF forecasting system. Bull Amer Meteor Soc 86(3):387

Anthes RA (2011) Exploring Earth's atmosphere with radio occultation: contributions to weather, climate, and space weather. Atmos Meas Tech 4(6):1077–1103

August T, Klaes D, Schlüssel P, Hultberg T, Crapeau M, Arriaga A, O'Carroll A, Coppens D, Munro R, Calbet X (2012) IASI on Metop-A: Operational Level 2 retrievals after five years in orbit. J Quant Spectrosc Radiat Transfer 113(11):1340–1371

Aumann HH, Chahine MT, Gautier C, Goldberg MD, Kalnay E, McMillin LM, Revercomb H, Rosenkranz PW, Smith WL, Staelin DH, Strow LL, Susskind J (2003) AIRS/AMSU/HSB on the aqua mission: design, science objectives, data products, and processing systems. IEEE Trans Geosci Remote Sens 41(2):253–264

Bauer P, Geer AJ, Lopez P, Salmond D (2010) Direct 4D-Var assimilation of all-sky radiances. Part I: Implementation. Quart J Royal Met Soc 136(652):1868–1885

Bodeker GE, Bojinski S, Cimini D, Dirksen RJ, Haeffelin M, Hannigan JW, Hurst DF, Leblanc T, Madonna F, Maturilli M, Mikalsen AC, Philipona R, Reale T, Seidel DJ, Tan DGH, Thorne PW, Vömel H, Wang J (2016) Reference Upper-Air Observations for Climate: From Concept to Reality. Bull Amer Meteor Soc 97(1):123–135

Bretherton CS, Uttal T, Fairall CW, Yuter SE, Weller RA, Baumgardner D, Comstock K, Wood R, Raga GB (2004) The Epic 2001 Stratocumulus Study. Bull Amer Meteor Soc 85(7):967–977

Bretherton CS, Blossey PN, Khairoutdinov M (2005) An Energy-Balance Analysis of Deep Convective Self-Aggregation above Uniform SST. J Atmos Sci 62(12):4273–4292

Brogniez H, Kirstetter PE, Eymard L (2013) Expected improvements in the atmospheric humidity profile retrieval using the Megha-Tropiques microwave payload. Quart J Royal Met Soc 139(673):842–851

Buehler SA, John VO (2005) A Simple Method to Relate Microwave Radiances to Upper Tropospheric Humidity. J Geophys Res 110(D2):D02,110

Buehler SA, Kuvatov M, John VO, Leiterer U, Dier H (2004) Comparison of Microwave Satellite Humidity Data and Radiosonde Profiles: A Case Study. J Geophys Res 109(D13):n/a–n/a

Clerbaux C, Boynard A, Clarisse L, George M, Hadji-Lazaro J, Herbin H, Hurtmans D, Pommier M, Razavi A, Turquety S, Wespes C, Coheur PF (2009) Monitoring of atmospheric composition using the thermal infrared IASI/MetOp sounder. Atmos Chem Phys 9(16):6041–6054

Dee DP, Uppala S (2009) Variational bias correction of satellite radiance data in the ERA-Interim reanalysis. Quart J Royal Met Soc 135(644):1830–1841

Dee DP, Uppala SM, Simmons AJ, Berrisford P, Poli P, Kobayashi S, Andrae U, Balmaseda MA, Balsamo G, Bauer P, Bechtold P, Beljaars ACM, van de Berg L, Bidlot J, Bormann N, Delsol C, Dragani R, Fuentes M, Geer AJ, Haimberger L, Healy SB, Hersbach H, Hólm EV, Isaksen L, Kållberg P, Köhler M, Matricardi M, McNally AP, Monge-Sanz BM, Morcrette JJ, Park BK, Peubey C, de Rosnay P, Tavolato C, Thepaut JN, Vitart F (2011) The ERA-Interim reanalysis: configuration and performance of the data assimilation system. Quart J Royal Met Soc 137(656):553–597

Edwards JM, Slingo A (1996) Studies with a flexible new radiation code. I: Choosing a configuration for a large-scale model. Quart J Royal Met Soc 122(531):689–719

Eriksson P, Buehler SA, Davis CP, Emde C, Lemke O (2011) ARTS, the atmospheric radiative transfer simulator, version 2. J Quant Spectrosc Radiat Transfer 112(10):1551–1558

Eyre JR, Kelly GA, McNally AP, Andersson E, Persson A (1993) Assimilation of TOVS radiance information through one-dimensional variational analysis. Quart J Royal Met Soc 119(514):1427–1463

Geer AJ, Bauer P, Lopez P (2010) Direct 4D-Var assimilation of all-sky radiances. Part II: Assessment. Quart J Royal Met Soc 136(652):1886–1905

Gorbunov ME, Benzon HH, Jensen AS, Lohmann MS, Nielsen AS (2004) Comparative analysis of radio occultation processing approaches based on Fourier integral

operators. Radio Sci 39(6):n/a–n/a

Hajj GA, Kursinski ER, Romans LJ, Bertiger WI, Leroy SS (2002) A technical description of atmospheric sounding by GPS occultation. J Atmos Solar-Terr Phys 64(4):451–469

Healy SB, Thepaut JN (2006) Assimilation experiments with CHAMP GPS radio occultation measurements. Quart J Royal Met Soc 132(615):605–623

Herbin H, Hurtmans D, Clerbaux C, Clarisse L, Coheur PF (2009) $H_2^{16}O$ and HDO measurements with IASI/MetOp. Atmos Chem Phys 9(24):9433–9447

Ho SP, Hunt D, Steiner AK, Mannucci AJ, Kirchengast G, Gleisner H, Heise S, von Engeln A, Marquardt C, Sokolovskiy S, Schreiner W, Scherllin-Pirscher B, Ao C, Wickert J, Syndergaard S, Lauritsen K, Leroy S, Kursinski ER, Kuo YH, Foelsche U, Schmidt T, Gorbunov M (2012) Reproducibility of GPS radio occultation data for climate monitoring: Profile-to-profile inter-comparison of CHAMP climate records 2002 to 2008 from six data centers. J Geophys Res 117(D18):n/a–n/a

Ho SP, Peng L, Anthes RA, Kuo YH, Lin HC (2015) Marine Boundary Layer Heights and Their Longitudinal, Diurnal, and Interseasonal Variability in the Southeastern Pacific Using COSMIC, CALIOP, and Radiosonde Data. J Climate 28(7):2856–2872

Hólm E, Andersson E, Beljaars A, Lopez P, Mahfouf JF, Simmons A, Thepaut JN (2002) Assimilation and modelling of the hydrological cycle: ECMWF2019s status and plans. Technical Memoranda 383

Immler FJ, Dykema J, Gardiner T, Whiteman DN, Thorne PW, Vömel H (2010) Reference Quality Upper-Air Measurements: guidance for developing GRUAN data products. Atmos Meas Tech 3(5):1217–1231

John VO, Holl G, Allan RP, Buehler SA, Parker DE, Soden BJ (2011) Clear-sky biases in satellite infrared estimates of upper tropospheric humidity and its trends. J Geophys Res 116(D14):1491

Kalman RE (1960) A New Approach to Linear Filtering and Prediction Problems. Transactions of the ASME–Journal of Basic Engineering 82(Series D):35–45

Kalman RE, Bucy RS (1961) New results in linear filtering and prediction theory. Transactions of the ASME–Journal of Basic Engineering 83(Series D):95–108

Kalnay E (2003) Atmospheric modeling, data assimilation and predictability. Cambridge university press

Kanamitsu M, Ebisuzaki W, Woollen J, Yang SK, Hnilo JJ, Fiorino M, Potter GL (2002) NCEP–DOE AMIP-II Reanalysis (R-2). Bull Amer Meteor Soc 83(11):1631–1643

Kirchengast G, Schweitzer S (2011) Climate benchmark profiling of greenhouse gases and thermodynamic structure and wind from space. Geophys Res Lett 38(13):L13,701–n/a

Kirchengast G, Schwärz M, Schwarz J, Scherllin-Pirscher B, Pock C, Innerkofler J, Proschek V, Steiner AK, Danzer J, Ladstädter F, Foelsche U (2016) The reference occultation processing system approach to interpret GNSS radio occultation as SI-traceable planetary system refractometer. Tech. rep.

Klaes KD, Cohen M, Buhler Y, Schlüssel P, Munro R, Engeln A, Clérigh E, Bonekamp H, Ackermann J, Schmetz J, Luntama JP (2007) An Introduction to

the EUMETSAT Polar system. Bull Amer Meteor Soc 88(7):1085–1096
Kleist DT, Ide K (2015) An OSSE-Based Evaluation of Hybrid Variational–Ensemble Data Assimilation for the NCEP GFS. Part I: System Description and 3D-Hybrid Results. Mon Wea Rev 143(2):433–451
Klinker E, Sardeshmukh PD (1992) The Diagnosis of Mechanical Dissipation in the Atmosphere from Large-Scale Balance Requirements. J Atmos Sci 49(7):608–627
Kobayashi S, OTA Y, HARADA Y, EBITA A, MORIYA M, ONODA H, ONOGI K, KAMAHORI H, KOBAYASHI C, ENDO H, MIYAOKA K, TAKAHASHI K (2015) The JRA-55 Reanalysis: General Specifications and Basic Characteristics. J Meteor Soc Japan 93(1):5–48
Kursinski ER, Gebhardt T (2014) A Method to Deconvolve Errors in GPS RO-Derived Water Vapor Histograms. J Atmos Oceanic Technol 31(12):2606–2628
Kursinski ER, Hajj GA, Schofield JT, Linfield RP, Hardy KR (1997) Observing Earth's atmosphere with radio occultation measurements using the Global Positioning System. J Geophys Res 102(D19):23,429–23,465
Kursinski ER, Syndergaard S, Flittner D, Feng D, Hajj GA, Herman B, Ward D, Yunck TP (2002) A Microwave Occultation Observing System Optimized to Characterize Atmospheric Water, Temperature, and Geopotential via Absorption. J Atmos Oceanic Technol 19(12):1897–1914
Lacour JL, Risi C, Clarisse L, Bony S, Hurtmans D, Clerbaux C, Coheur PF (2012) Mid-tropospheric δD observations from IASI/MetOp at high spatial and temporal resolution. Atmos Chem Phys 12(22):10,817–10,832
Ladstädter F, Steiner AK, Schwärz M, Kirchengast G (2015) Climate intercomparison of GPS radio occultation, RS90/92 radiosondes and GRUAN from 2002 to 2013. Atmos Meas Tech 8(4):1819–1834
Li Y, Kirchengast G, Scherllin-Pirscher B, Schwärz M, Nielsen JK, Wee TK, Ho SP, Yuan YB (2016) A new algorithm for the retrieval of atmospheric profiles from GNSS radio occultation data in moist air conditions. J Geophys Res
Liao M, Zhang P, Yang GL, Bi YM, Liu Y, Bai WH, Meng XG, Du QF, Sun YQ (2016) Preliminary validation of the refractivity from the new radio occultation sounder GNOS/FY-3C. Atmos Meas Tech 9(2):781–792
Liu CL, Kirchengast G, Syndergaard S, Kursinski ER, Sun YQ, Bai WH, Du QF (2017) A review of low Earth orbit occultation using microwave and infrared-laser signals for monitoring the atmosphere and climate. Adv Space Res
Mears CA, Wang J, Smith D, Wentz FJ (2015) Intercomparison of total precipitable water measurements made by satellite-borne microwave radiometers and ground-based GPS instruments. J Geophys Res 120(6):2492–2504
Osher S, Burger M, Goldfarb D, Xu J, Yin W (2005) An Iterative Regularization Method For Total Variation-Based Image Restoration. Multiscale Model Simul 4(2):460–489
Parker WS (2016) Reanalyses and Observations: What's the Difference? Bull Amer Meteor Soc 97(9):1565–1572
Rieckh T, Anthes R, Randel W, Ho SP, Foelsche U (2016) Tropospheric dry layers in the Tropical Western Pacific: Comparisons of GPS radio occultation with multiple data sets. Atmos Meas Tech Discuss pp 1–22

Rodwell MJ, Palmer TN (2007) Using numerical weather prediction to assess climate models. Quart J Royal Met Soc 133(622):129–146

Schmetz J, Pili P, Tjemkes S, Just D, Kerkmann J, Rota S, Ratier A (2002) An introduction to Meteosat Second Generation (MSG). Bull Amer Meteor Soc 83(7):977–992

Schneider M, Hase F (2011) Optimal estimation of tropospheric H_2O and δD with IASI/METOP. Atmos Chem Phys 11(21):11,207–11,220

Schreiner WS, Rocken C, Sokolovskiy S, Hunt D (2009) Quality assessment of COSMIC/FORMOSAT-3 GPS radio occultation data derived from single- and double-difference atmospheric excess phase processing. GPS Solut 14(1):13–22

Shi L, Bates JJ (2011) Three decades of intersatellite-calibrated High-Resolution Infrared Radiation Sounder upper tropospheric water vapor. J Geophys Res 116(D4):D04,108–n/a

Sokolovskiy S, Schreiner W, Zeng Z, Hunt D, Lin YC, Kuo YH (2014) Observation, analysis, and modeling of deep radio occultation signals: Effects of tropospheric ducts and interfering signals. Radio Sci 49(10):954–970

Steiner AK, Lackner BC, Ladstädter F, Scherllin-Pirscher B, Foelsche U, Kirchengast G (2011) GPS radio occultation for climate monitoring and change detection. Radio Sci 46(6):115

Steiner AK, Hunt D, Ho SP, Kirchengast G, Mannucci AJ, Scherllin-Pirscher B, Gleisner H, von Engeln A, Schmidt T, Ao C, Leroy SS, Kursinski ER, Foelsche U, Gorbunov M, Heise S, Kuo YH, Lauritsen KB, Marquardt C, Rocken C, Schreiner W, Sokolovskiy S, Syndergaard S, Wickert J (2013) Quantification of structural uncertainty in climate data records from GPS radio occultation. Atmos Chem Phys 13(3):1469–1484

Stevens B, Farrell D, Hirsch L, Jansen F, Nuijens L, Serikov I, Brügmann B, Forde M, Linne H, Lonitz K, Prospero JM (2016) The Barbados Cloud Observatory: Anchoring Investigations of Clouds and Circulation on the Edge of the ITCZ. Bull Amer Meteor Soc 97(5):787–801

Stevens B, Brogniez H, Kiemle C, Lacour JL, Crevoisier C, Kiliani J (2017) Structure and Dynamical Influence of Water Vapor in the Lower Tropical Troposphere. Surv Geophys 105(3):270

Tobin I, Bony S, Roca R (2012) Observational Evidence for Relationships between the Degree of Aggregation of Deep Convection, Water Vapor, Surface Fluxes, and Radiation. J Climate 25(20):6885–6904

Trenberth KE, Fasullo JT, Mackaro J (2011) Atmospheric moisture transports from ocean to land and global energy flows in reanalyses. J Climate 24(18):4907–4924

Uppala SM, Kållberg PW, Simmons AJ, Andrae U, Bechtold Vd, Fiorino M, Gibson JK, Haseler J, Hernandez A, Kelly GA, others (2005) The ERA-40 re-analysis. Quart J Royal Met Soc 131(612):2961–3012

Vial J, Bony S, Stevens B, Vogel R (2017) Mechanisms and Model Diversity of Trade-Wind Shallow Cumulus Cloud Feedbacks: A Review. Surv Geophys 36(1):73

Wang X, Parrish D, Kleist D, Whitaker J (2013) GSI 3DVar-Based Ensemble–Variational Hybrid Data Assimilation for NCEP Global Forecast System: Single-Resolution Experiments. Mon Wea Rev 141(11):4098–4117

Wing AA, Emanuel K, Holloway CE, Muller C (2017) Convective Self-Aggregation in Numerical Simulations: A Review. Surv Geophys 27(32):4391

Xie F, Wu DL, Ao CO, Mannucci AJ, Kursinski ER (2012) Advances and limitations of atmospheric boundary layer observations with GPS occultation over southeast Pacific Ocean. Atmos Chem Phys 12(2):903–918